

Fluid-Driven Soft CoboSkin for Safer Human–Robot Collaboration: Fabrication and Adaptation

Wenzheng Heng, Geng Yang,* Gaoyang Pang, Zhiqiu Ye, Honghao Lv, Juan Du, Guodong Zhao, and Zhibo Pang

In human–robot collaboration, the wrapping material on robots is not only required to have the sensing ability to adapt to the external environment but also need to have the function of cushioning the collision between human and robot. Herein, a fluid-driven soft robot skin with sensing and actuating function is successfully applied to a collaborative robot and working well with the host robot. The skin is an integration of sponge force sensors and pneumatic actuators. By altering the internal air pressure in pneumatic actuators, the developed robot skin can provide more than ten times tunable stiffness and sensitivity. In addition, the skin can reduce the peak force of the collision and achieve the actuating function. Using three-dimensional printing and computer-aided design, the skin is fabricated and attached to a collaborative robot conformally. Drawing upon the data acquisition and control system, the experiment for illustrating the applications of the CoboSkin is successfully performed. The skin provides the robot with multi-functions, which are similar to the human muscle and skin attached to human bones. By mimicking human skin and muscle with tactile sensing function and stiffness tuning function, CoboSkin can enhance the adaptability of the robot to human daily life.

1. Introduction

Recently, the collaborative robot (Cobot) has become an emerging subfield in robotics, which significantly expands the applications of robots, such as smart manufacturing,^[1] professional service,^[2] and health care.^[3] Thanks to the development of sensing technology,^[4] data analysis,^[5] and control science,^[6] the adaptability of Cobot to complex unconstructed environments has enhanced hugely. However, in human–robot collaboration (HRC), the further integration of Cobots and human daily life still needs more advanced devices or intelligent systems to assist Cobots to satisfy several essential requirements, such as security assurance,^[7] information perception,^[8] and emotional communication.^[9]

The paramount differences between Cobots and traditional robots lie in sensor systems and safety strategies. Examples of sensing systems of Cobots include computer vision,^[10] proximity sensing,^[9] and tactile interaction.^[11] Compared with Cobots which solely obtain information from cameras, Cobots with tactile sensing ability are more capable of cooperating with humans in complex environments, such as places with dim lighting, smoke-filled areas, or visual blind spots.^[12] Thus, robot skin plays an essential role in physical human–robot interaction, which includes tactile sensing and buffering capacity. From the perspective of tactile sensing, robot skin to endow host Cobots with tactile sensing function to satisfy the perceptual requirements of robots' adaptation in unstructured and constrained environments has become exceedingly heated research interdisciplinary in robotics.^[13] In addition, the tactile sensing function of robot skin also provides more opportunities for Cobots to get control information from the human partner in HRC, which will definitely enhance the safety flexibility and efficiency of HRC. Moreover, tactile sensing of the robot also makes it possible for human and robot emotional interaction through physical touching. Collision detection and buffering are also important functions of robot skin in HRC. There are two ways for robot skin to realize collision detection: One is to use viscoelastic material as raw material of sensors or substrate material of pressure sensors to cushion the collision and detect the peak force of a collision;^[14] the other is to use flexible sensors attached to the airbag structure to detect the peak force of a collision.^[7,15]

W. Heng, Prof. G. Yang, G. Pang, Z. Ye, H. Lv
State Key Laboratory of Fluid Power and Mechatronic Systems
School of Mechanical Engineering
Zhejiang University
Hangzhou 310027, China
E-mail: yanggeng@zju.edu.cn

Dr. J. Du
First Affiliated Hospital of Zhejiang University School of Medicine
Zhejiang University
Hangzhou 310027, China

Dr. G. Zhao
School of Engineering
University of Glasgow
Glasgow G12 8LT, UK

Dr. Z. Pang
Automation Technology
ABB Corporate Research Sweden
Vasteras 72178, Sweden

 The ORCID identification number(s) for the author(s) of this article can be found under <https://doi.org/10.1002/aisy.202000038>.

© 2020 The Authors. Published by WILEY-VCH Verlag GmbH & Co. KGaA, Weinheim. This is an open access article under the terms of the Creative Commons Attribution License, which permits use, distribution and reproduction in any medium, provided the original work is properly cited.

DOI: 10.1002/aisy.202000038

However, there are two challenges to the application of robot skin. First, the safety of Cobot is not always simply guaranteed by leveraging traditional robot skin, because some robot skin are made of rigid components or the thicknesses of flexible robot skin in previous work is generally so thin that does not have the ability to cushion unintended contacts between human and robot.^[16] To avoid hazardous collision between humans and robots, an ocean of safety strategies have been proposed, such as compliant components,^[17] lightweight design,^[18] and soft padding material.^[19] Limitations of the first two strategies are obvious; for instance, the limited payload and low positioning accuracy.^[20] The traditional soft padding layer being wrapped around critical parts of the robot in existing industrial practice do not have sensing function, which confines the information perception ability of robots.^[21] To address this challenge, we got inspiration from natural skin and muscle which can help creatures to sense the external world and resist dangerous collision by stiffening and softening. Our previous work has proposed and fabricated a novel fluid-driven soft robot skin with sensing and actuating functions for safer HRC, illustrating that the skin has the basic feasibility of sensing and buffering collision in the state of the plane structure.^[22] To make the robot's whole body have anticollision and sensing functions similar to that of natural muscles or skin, another challenge in applying soft skin to robot bodies is to follow the complex contour and various shapes on the robot, which is not well-addressed and illustrated in that article.

There are several methods to tackle the integration in previous research. Qiu et al.^[23] proposed a kind of self-conformable smart skin with sensing and variable stiffness functions, which could conform to the shape of some surfaces with simple geometries. However, a lot of existing commercial robots have various contours, which are much more complex than simple geometries. To make robot skin easier to attach conformally on robots and enhance the safety of HRC, some rigid devices integrated with various sensors have been fabricated into small units.^[13] However, at present, the spatial resolution of the device is not enough to fit the complex surface of current commercial robots. Another solution is adopting soft material in robot skin. Nowadays, most prototypes are made of soft,^[24] flexible,^[25] or even stretchable materials.^[26] Nevertheless, the flexible robot skin is also difficult to conformally attach to the various contours of commercial robots.

Building upon the fundamental physical concepts, materials, and fabrication process of collaborative robot skin (CoboSkin) introduced in our previous work,^[22] in this article, we proposed a prototyping method for the integration of Cobot and CoboSkin, and further explored the actuating function of the CoboSkin. The fabricated fluid-driven CoboSkin is able to be conformally integrated onto the complex contour of the host Cobot. The developed CoboSkin is capable of endowing a Cobot with sensing and actuating functions for safer HRC. There are two kinds of functional units distributed evenly in a horizontal direction and encapsulated through the foaming process, providing CoboSkin with sensing and actuating functions simultaneously. From the perspective of sensors, the parallel distribution structure of sensors and actuators in a vertical direction can actively influence the difficulty of the compressive deformation of the piezoresistive sensor through verifying the stiffness of actuators, thereby altering the sensitivity and detection range of CoboSkin.

From the perspective of actuators, first, the CoboSkin can achieve the stepless recovering and lifting function. Second, according to the research on the relationship between the peak impact force and interface stiffness during collisions, the CoboSkin can reduce the peak force by adjusting the stiffness of actuators. This article departs from our previous work by 1) proposing new methods for the fabrication and integration of CoboSkin, enabling CoboSkin to be installed to the complex contour and various shapes on the robot; 2) illustrating the new function of a shape recovery actuating enabled by pumping high-pressure gas into actuators in the CoboSkin; and 3) envisioning and exploring the bionic design of CoboSkin, which is inspired by the human body, such as the human muscle and human skin. From the perspective of new visions in a bionic design inspired by the human body, the proposed CoboSkin is composed of piezoresistive sensing cells and pneumatic actuating cells. Piezoresistive sensing cells enable the CoboSkin to obtain on-site tactile data in real time, which is inspired by human skin. Muscle-inspired pneumatic actuating cells endow the CoboSkin with controllable stiffness by adjusting internal air pressure levels.

The rest of the article is organized as follows. The bionic inspiration of this design, characteristics of components in CoboSkin are described in Section 2.1. Then, the prototyping of the CoboSkin and the sensing and actuating functions of CoboSkin are experimentally demonstrated in Section 2.2. Finally, the adaptation of mechanical design, the integration of the control system, and the minimum detection force comparison are illustrated in Section 2.3., followed by a conclusion section (Section 3) and an experimental section (Section 4).

2. Results and Discussion

2.1. Generalization of the CoboSkin by Bionic Design

2.1.1. Inspiration of Human Body

A lot of daily behaviors of creatures are accompanied by changes in the stiffness of soft structure on their bodies in nature: the elephant with its trunk is very dexterous when soft, while it also can transmit very high forces when it is hard.^[27] In addition, the squid with its tentacles and the octopus is able to selectively stiffen parts of its arms to use them as a modifiable skeleton for both quick escape and fierce predation.^[28] The stiffness of tongues could change in different situations, such as eating and speaking.^[29,30] Stiffness turning is a kind of environmental adaptation of biological behavior which can be effectively beneficial for creatures' interaction with the environment. Natural softness endows dexterity and safe interactions, but stiffening is required to increase the forces transferred to the environment when necessary.^[27]

Here, the CoboSkin integrated on robot just mimic the phenomenon of muscle stiffness changing when humans encounter impact from external objects or exert force. They instinctively react defensively by tightening muscles for increasing their stiffness. In this way, much of the impact energy will be absorbed by the tensed muscle to reduce damage to bones and other vital organs. By stiffening our muscles, we can reduce damage to the human body, the environment, and the object. In another aspect,

the harder our muscles are, the more force they can carry, and the more force we can perceive consciously.

Robots also need bionic devices to cover themselves, which should be similar to human muscles and skin, as shown in **Figure 1a**. By leveraging this crucial instinctive reaction of the human body, we designed a kind of stiffness variable pneumatic actuating cell to act as muscles for reducing the impact force in a human–robot collision, as shown in **Figure 1b**. On one hand, it can reduce the damage to robots. On the other hand, the peak impact force of the collision toward the human body also declines. Moreover, sponge force sensors (piezoresistive sensing cells) act as force receptors on the human skin surface to detect static and dynamic collision force for host robots in HRC. Through a vertical parallel combination of these two kinds of function units, the external force applied on robot skin is divided by them. Thus, CoboSkin overturned the traditional sensor concept: its detection range and sensitivity can be changed by altering internal air pressure in actuating cells based on the target detection force. Although the CoboSkin have detection dead zone on pneumatic actuators, there are several ways to solve the problem. For instance, making all these functional units smaller, arranging all these functional units more tightly, or integrating the two kinds of functional units into one unit.

2.1.2. Piezoresistive Sensing Cell

Wu et al.^[31] recently reported a kind of large-area, cost-effective, and versatile pressure sensor which is made of carbon black (CB) and polyurethane (PU) sponge. Many of the researches in sponge^[32] and carbon-related sensitive functional materials^[33] in the last five years have exhibited that these two kinds of materials have many favorable characteristics, such as light weight, high sensitivity, and low cost, which are well suited as raw materials for flexible sensors. Most importantly, the sponge is widely used in robot components, due to the characteristics of viscoelastic material which can effectively absorb the energy of shock and reduce the peak force of a collision. Many commercial Cobots adopt this material as a wrapping layer, such as ABB “YuMi” robot. Thus, the sponge with a sensing function is a promising material to cover Cobots. Here, we adopted PU sponge and CB as raw materials to fabricate sponge-based

piezoresistive sensing cells (See more details of the fabrication process in Section 4).

In this section, the piezoresistive properties of flexible porous sponge sensing cells are described. The electrical characteristics of sensing cells under force are shown in **Figure 2**. As shown in **Figure 2a**, we chose copper needles as the electrodes for the sensing cell and inserted them into the sponge sensing cell to detect the electric current in the sensing cell upon a constant voltage. The current variation ratio $((I - I_0)/I_0)$, where I_0 and I denote the measured current without and with applied pressure, respectively) of one sensing unit was calculated on the basis of measured values and were plotted as a function of the applied force, as shown in **Figure 2b**. The pressure sensitivity S can be defined as the slope of curves in **Figure 2b ($S = \delta((I - I_0)/I_0)/\delta \cdot F$, where F denotes the applied force). In the compressing process, due to the increased contact points among the inner backbones of the sensing cell, the resistance of the sensing cell constantly decreased. In addition, to demonstrate the stability of the sensing cell, we loaded stepped force on it at a constant loading speed of 5 mm min^{-1} . **Figure 2c** shows the electric response of the sensing cell. It can be seen that after each step loading, the electric current in the sensor can be kept stable to a certain level. After all the external forces were removed, the electric current in the sensor returned to its original value, which means that the initial resistance of the sensing cell does not change in the loading and unloading experiment. The responsive behaviors of the sensing cell to small repeated compressive triangle force variations were recorded. As shown in **Figure 2d**, stable and continuous electric current responses could be observed. As the compressive force increased from 0.25 to 1 N, the intensity of current variation ratios became higher. Moreover, the variation range of this experiment is almost in line with the experiment in **Figure 2c**, and the difference is around 10% due to the unstable electrical connection. As shown in **Figure 2e**, during 2000 loading–unloading cyclic tests at 1 N, the responsive signal output kept consistent. The excellent reproducibility of this sensor implied its reliability and durability.**

2.1.3. Pneumatic Actuating Cell

With the development of pneumatic technologies, air pumps are becoming more portable, lightweight, and silent to use.^[34]

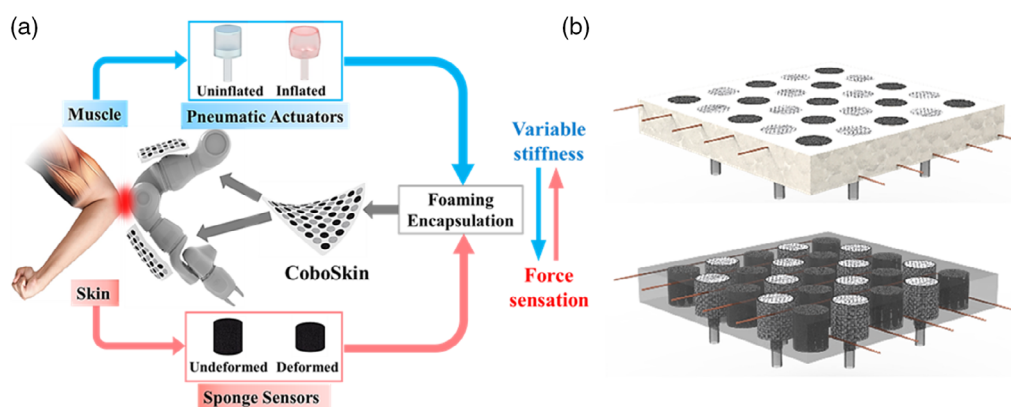


Figure 1. Bionic design of CoboSkin. a) The inspiration of the human body. b) Appearance structure and perspective of CoboSkin.

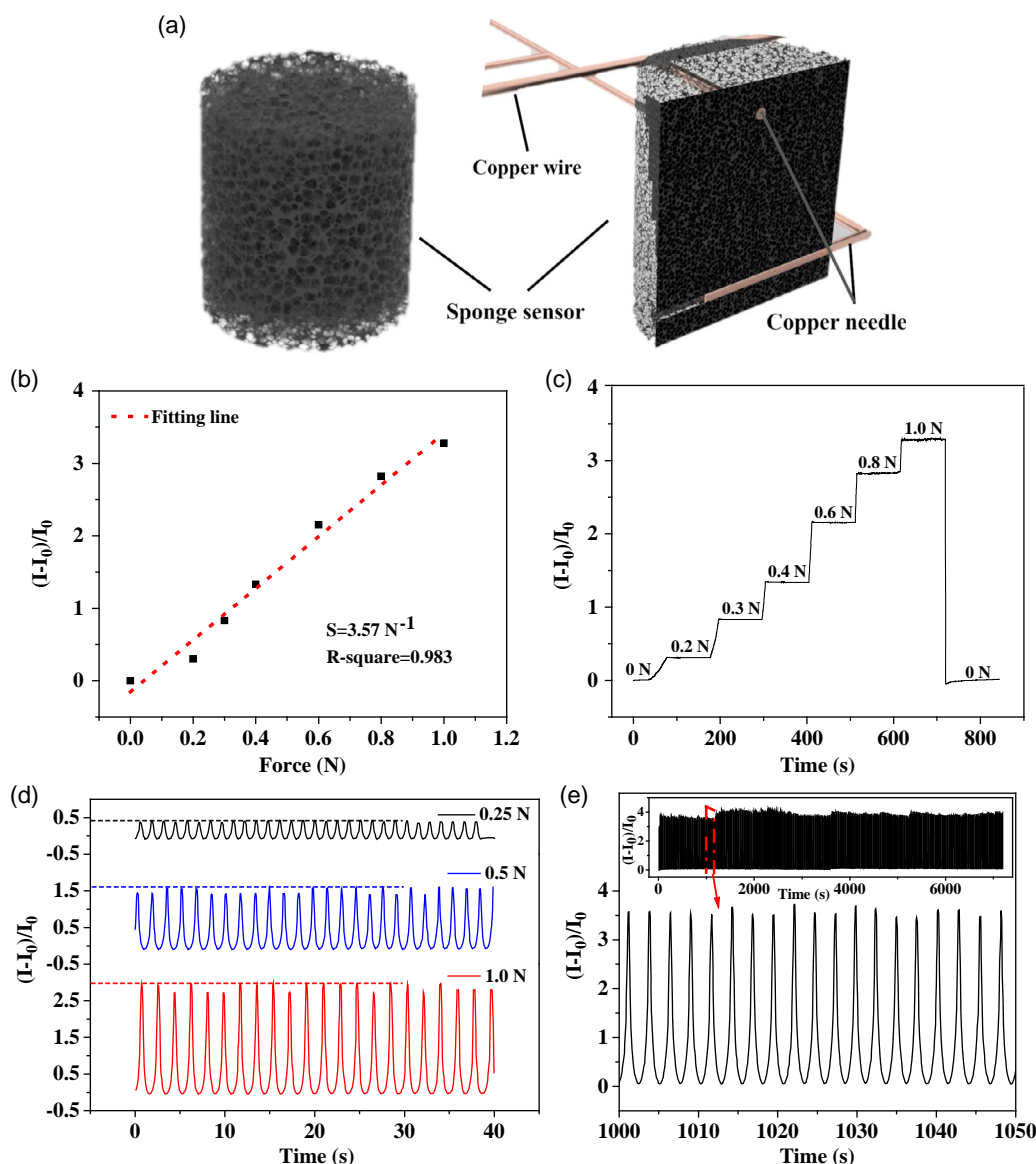


Figure 2. Piezoresistive sensing cell of CoboSkin. a) Schematics illustration of a sponge force sensor. b) Relative current change of a sponge force sensor versus compressive force. c) The responsive current curve of a sponge force sensor under step loading–unloading test. d) Repeated compressing tests of a sponge force sensor at different external force levels. e) Reproducibility test of a sponge force sensor for 2000 cycles at 1 N external force.

In addition to the air pump, chemical reactions can also provide a gas source as a method that can be stored and carried easily without the use of an external air pump.^[35] The aforementioned technologies have been driving the pneumatic applications in robotics; many robots also have corresponding air path inside to satisfy the requirement of pneumatic actuators, such as soft robot hand, sucker.^[36]

In high-speed impacts, timely inflating of automobile airbags can effectively reduce the damage caused by collision to the human body, which proves that pneumatic airbag can slow down collision to certain extent, and absorb the collision energy, thereby reducing the peak force of the collision. A lot of related researches also demonstrated that attaching inflatable modules on robots is an extremely effective way to prevent collision

damage.^[37,38] However, the structure of airbags in cars and inflatable modules in existing research is not totally suitable for robot applications, because the expansion of this structure will interfere with the movements of the robot, which will reduce the working ability and application of robots. A device which stiffens possibly without much deformation is a better choice for robot applications.

Here, we got inspiration from automobile tires and constructed the pneumatic actuating cell into a double layers' structure. The detailed fabrication process of pneumatic actuating cells is introduced in Section 4. As shown in **Figure 3a**, the internal layer of the pneumatic actuating cell was made of silicon rubber, the function of which is to ensure no air leakage and keep high-pressure gas inside it. At the same time, silicon

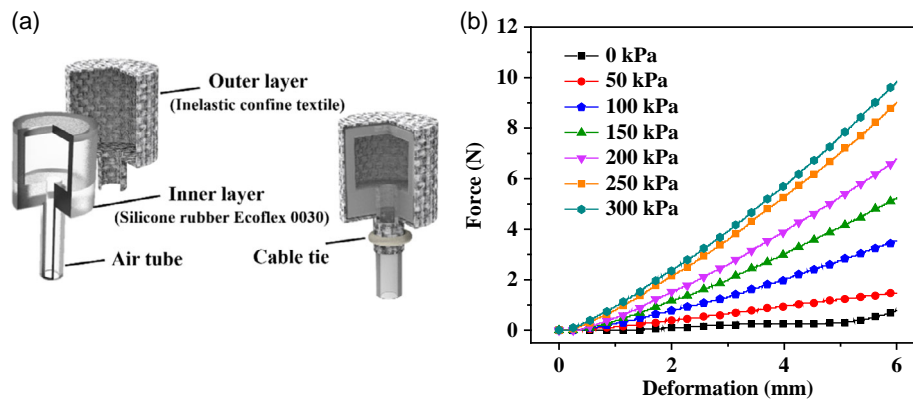


Figure 3. The pneumatic actuator of CoboSkin. a) Schematic illustration of a pneumatic actuator sensor. b) Calibration of variable stiffness of the pneumatic actuator with seven internal pressure levels.

rubber, as a kind of soft viscoelastic material, is a common material used in human–robot interaction and safe collaboration.^[14,39] The external layer of the actuating cell was a confining layer to enhance the structural strength and limit the deformation of the pneumatic actuating cell. To achieve aforementioned functions, we chose inelastic nylon textile, which is easy to fold, but quite hard to expand. Therefore, the whole function of this actuating cell is extremely similar to that of natural muscle; when the stiffness of muscle changes, its appearance changes only slightly.

To demonstrate the effect of stiffness changes, an experiment was performed to detect the stiffness of actuating cell by setting several specific internal air pressures. Figure 3b shows the result, as the internal air pressure increased from 0 to 300 kPa, the stiffness ($k = \delta F / \delta x$, where F denotes the applied force, x denotes the compressive deformation) of pneumatic actuating cell also rose steadily from 0.13 to 1.64 N mm⁻¹, which indicates that the hardest actuating cell (internal air pressure: 300 kPa) is 12 times harder than the softest one (internal air pressure: 0 kPa). The appearance deformation data of the actuating cell is shown in Table 1. The main deformation changed between 0 and 50 kPa, which is in line with our cognition. Internal gas will expand until the external layer confines it. This experiment demonstrated that with the increase in the internal air pressure, the stiffness of the actuating cell also increased without large deformation.

2.2. Fabrication and Characterization of the CoboSkin

2.2.1. Prototyping of the CoboSkin

There are several ways to fabricate components, such as emerging additive manufacturing,^[40] traditional injection molding,^[41]

Table 1. Basic characteristics of pneumatic actuator varying with internal air pressure.

Internal air pressure [kPa]	0	50	100	150	200	250	300
Height [mm]	10	8.7	8.5	8.5	8.5	8.5	8.5
Max diameter ^{a)} [mm]	10	12.0	12.2	12.3	12.3	12.3	12.3

^{a)}The largest circular diameter of the section on the pneumatic actuator.

and subtractive manufacturing.^[42] The first two methods are widely used in the fabrication of flexible components. Nowadays, with the development of computer-aided design and 3D printing technology, the injection molds are much easier to design and fabricate than ever before. In the prototyping of the CoboSkin, we first designed the related molds on software, then used the 3D printing technology to make molds for both actuating cells molding and CoboSkin encapsulation molding. Finally, we used the silicon rubber as the raw material of actuating cells, commercial PU sponge as the raw material of sensing cells, and PU foaming sponge as the encapsulation material of functional units in CoboSkin.

In this section, we take the CoboSkin to one link of YuMi dual arms as an example to illustrate the achievability of the CoboSkin prototype. First, we designed four components of the prototyping fabrication process, including CoboSkin carrier, outer mold, fixed bracket, and foaming box, as shown in Figure 4a. CoboSkin carrier acted as the connector between CoboSkin and robot, mimicking the bone of a robot with CoboSkin growing on it. The design of the CoboSkin carrier should be specific to the contour of the robot arm, and the reason is explained in detail in Section 2.3.1. The purpose of the outer mold is to confine the foaming process and mold the shape of CoboSkin. The fixed bracket and foaming box are used together to contain foaming material and served as a foaming reaction vessel. All these four components can be installed together to finish the prototyping process, as shown in Figure 4b. After peeling off, a complete CoboSkin is formed on the CoboSkin carrier, as shown in Figure 4c. The thickness of CoboSkin is mainly up to the height of functional units. So, we can fabricate smaller actuators and thinner sensing unit, and foam them in a thinner mold to reduce the thickness of CoboSkin.

2.2.2. Active Sensing Function

The sensitivity and detection range of a traditional sensor are constant, which means users need to find appropriate sensors with desirable detection range and sensitivity, according to application scenarios. This greatly limits the scope of the sensor. In this article, we named this kind of traditional sensor a

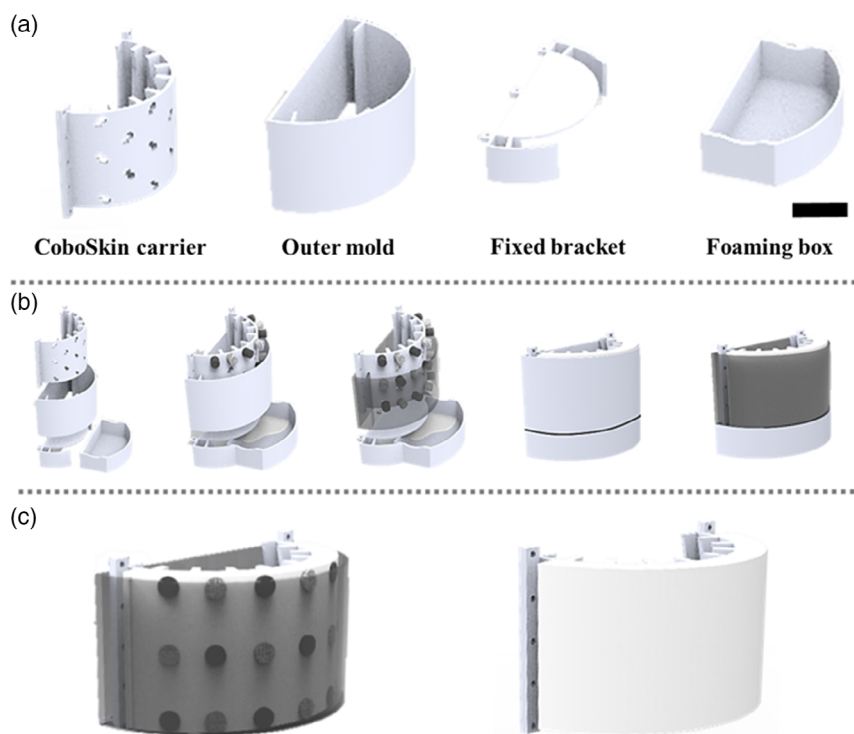


Figure 4. Prototyping of the CoboSkin. a) 3D printed models. Scale bar 5 cm. b) Installation and foaming process. c) Lateral and perspective view of the CoboSkin.

“passive sensor”, whose output data only depends on an external force. Nevertheless, the novel design of CoboSkin provides a new scope for sensors, which could alter the detection range and sensitivity through actively changing other related parameters to enhance the adaptability of sensors. Here, we name CoboSkin as an “active sensor”. Clearly, “active sensor” is more suitable for Cobots to precept external information because most Cobots mainly work in an unconstructed complex physical environment and face the unpredictable external force to detect.

To intuitively show the effect of internal air pressure on the sensitivity and detection range, we calibrated the electric

characteristics of CoboSkin with seven different pressure levels. **Figure 5a** shows the calibration curves of CoboSkin with different internal air pressures. CoboSkin with small internal air pressure exhibits relatively higher sensitivity. This is because CoboSkin with smaller internal air pressure is easier to deform under external force, whereas the deformation gets saturated gradually at high external force. In contrast, CoboSkin with larger internal air pressure exhibited lower sensitivity but a broader working range. This is due to the fact that CoboSkin with larger internal air pressure is more resistant to force-induced deformation.

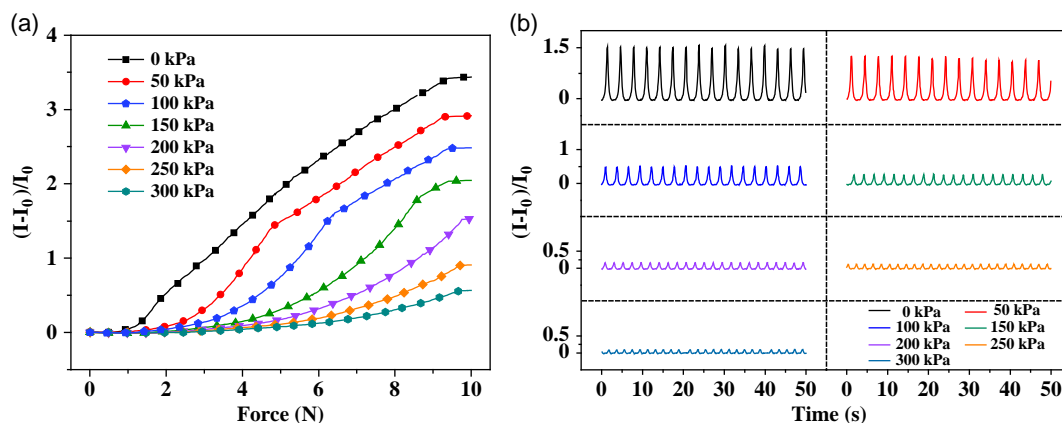


Figure 5. Piezoresistive properties of CoboSkin. a) Relative current change in CoboSkin versus compressive force with seven internal pressure levels. b) Repeated compressing tests of CoboSkin at the same force (5 N) with different internal air pressure.

Furthermore, the resistive responses of CoboSkin with different internal air pressures to the same repeated applied force loading and unloading were recorded and plotted in Figure 5b. It clearly shows that with the change in internal air pressure, the initial current, or in other words, the initial resistance of CoboSkin still keeps stable, whereas the dynamic response sensitivity changed hugely. CoboSkin without internal air pressure, whose current variation ratio range is 0–1.5, is most sensitive to a dynamic external force. As shown in the previous section (Section 2.1.3.), the higher internal air pressure is, the harder CoboSkin is, which means CoboSkin with higher internal air pressure will be more difficult to deform. The experimental results also demonstrated that, and the current variation ratios range of CoboSkin with 300 kPa internal air pressure is only 0–0.1, which is 15 times smaller than the output signal range of CoboSkin without internal air pressure. This experiment illustrated that we could alter the sensitivity of CoboSkin by actively changing the internal air pressure. Meanwhile, the initial resistance of CoboSkin can remain unchanged under different internal air pressures.

2.2.3. Pneumatic Actuating Function

The actuating ranges of traditional pneumatic actuators are generally large, and the control precisions of them are low.^[43] Slow actuation and precise positioning are necessary for the robot to perform delicate tasks. CoboSkin has an active ability to recover its shape by pumping high-pressure gas into actuating cell stepless. With this ability, CoboSkin is able to achieve simple actuating effects with controllable speed and precision, such as supporting and clamping. In this article, we designed an

experiment to demonstrate the supporting function and related sensing response of CoboSkin.

To illustrate the supporting and lifting function of CoboSkin, a ball screw platform was set up. As shown in Figure 6a, the plate connected with the ball screw was supported and lifted by one CoboSkin unit. The experiment results with different internal air pressures were shown in Figure 6b. Here, we pumped four different pressures compressive gas into the CoboSkin unit. When there was no compressive gas in the CoboSkin unit, the deformation of the unit was the largest one. With the increase in internal air pressure, the airbag gradually expands, and its load area decreases, so that the internal and external forces were balanced, and the height of the CoboSkin unit also increases. When the air pressure reaches 300 kPa, CoboSkin is basically in a state of no deformation, which means that the lifting function of CoboSkin has an upper limit. This supporting and lifting function of CoboSkin can provide the robot with a stepless motion method with pumping different pressure compressive gas into it, which can effectively lift objects at a small distance. Moreover, this experiment can also explain the principle why the sensing output could be changed by altering the internal air pressure. The detailed experiment was recorded as video 1, Supporting Information.

Figure 7a shows the schematics (front view and top view) and photography of the experimental setup for testing the actuating and related sensing response of CoboSkin. A pathway for steel ball was fixed on the platform to monitor platform tilt. The read-out circuit of the CoboSkin is used to read the electrical parameters of the sensing cell in the CoboSkin, so as to record the sensing response. In this experiment, four CoboSkin units supported a plastic plate with counterweights on it. Each CoboSkin unit includes one pneumatic actuating cell and one

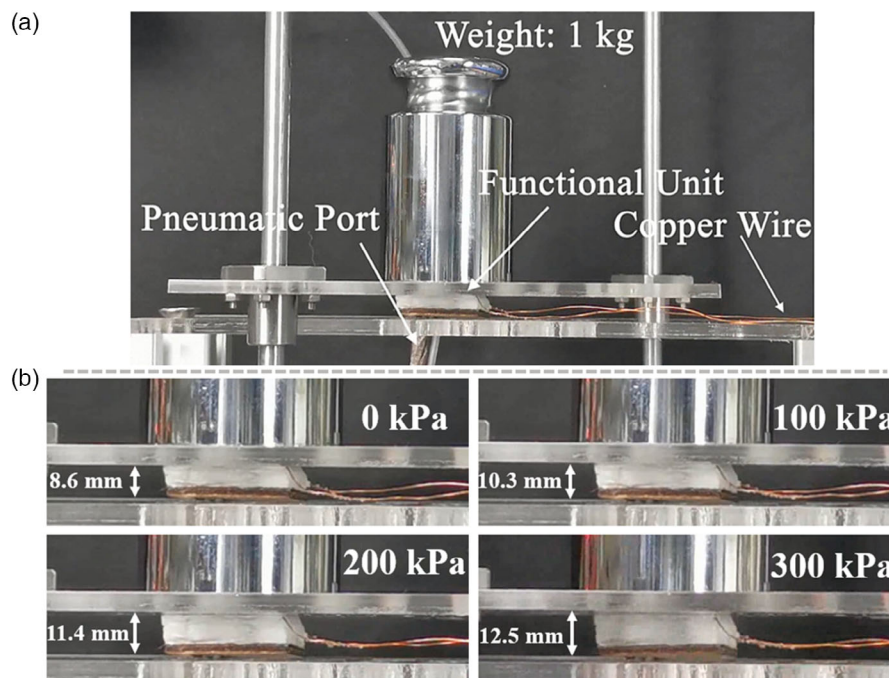


Figure 6. CoboSkin unit operates as a lifting actuator. a) Photography of the experimental setup for testing the supporting and lifting function of CoboSkin. b) CoboSkin lifting effect under different pressures (0, 100, 200, and 300 kPa).

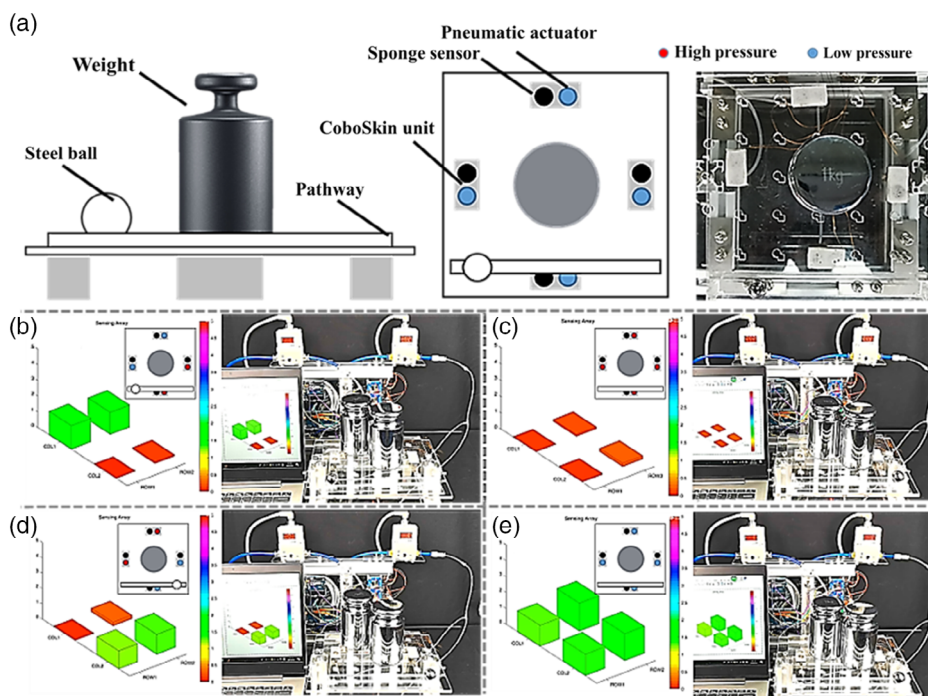


Figure 7. Actuating and related sensing response of CoboSkin. a) Schematics (front view and top view) and photograph of the experimental setup for testing the actuating and related sensing response of CoboSkin. b) The sensing response of CoboSkin and the tilt of the plate, when the internal air pressure changes in four CoboSkin units supporting the plate. High pressure (200 kPa): right and down; low pressure (0 kPa): left and up; ball position: left. c) High pressure (200 kPa): all, ball position: right. d) High pressure (200 kPa): right and down; low pressure (0 kPa): left and up; ball position: right. e). Low pressure (0 kPa): all; ball position: right.

piezoresistive sensing cell. Four situations under different pressure are shown in Figure 7d,e. First, due to the weight of counterweights, these four CoboSkin units without internal air pressure have been squashed several millimeters. As shown in Figure 7e, the corresponding sensing output is also high. After pumping high-pressure compressed gas into all four actuators in CoboSkin, the plate with counterweights on CoboSkin units was lifted, and these four CoboSkin units almost returned to the original shape. Thus, Figure 7c shows the output data of sensing units in CoboSkin under this state was much smaller than the former state. Furthermore, the plate tilt also could be altered by controlling the air pressure in these four supporting CoboSkin units. When the actuators were actuated as in Figure 7b,d, the plate tilt will be changed due to the ununiformed deformation of these CoboSkin units. The steel ball on the plate could reflect the tilt visually. In Figure 7b, the left and lower units were filled with high-pressure gas, so the plate tilted up to the right, which was illustrated by the position of the steel ball. At the same time, the sensing response of four units also in line with the actuating effect. Figure 7d shows the opposite situation. The detailed experiment was recorded as video 1, Supporting Information.

Previously, there were many pieces of research on the combination of sensors and actuators, which were usually used for visual feedback or safe human–robot interaction. Robinson et al.^[44] proposed a highly extensible sensing skin that they integrated with soft, actuating cells via a 3D printing technique called direct ink writing. This skin enables soft machines to

sense external stimuli as well as their shape, thus creating a device that has both tactile and kinesthetic sensations. Kim et al.^[15] proposed a soft inflatable module with self-contained sensing to avoid dangerous contact between humans and robots. All these devices have deformable components, which interfere with the initial resistance or capacitance of sensors on them and bring difficulties in decoupling the sensing data. The design of CoboSkin allows the actuator to change in stiffness but not in deformation, when the CoboSkin is not loaded with external force. The principle of the actuating unit in CoboSkin is similar to that of tires. Its external in-elastic fabric can limit the deformation which avoids the effect of the stiffness change on the baseline value of the sensor.

The safety effect of CoboSkin with different internal air pressure was illustrated via collision tests. To evaluate the safety performance of the CoboSkin, we prepared a setup for collision testing. CoboSkin was fixed on a revolute joint linkage structure connected to a tension spring. By pulling and releasing the rotatable linkage from different initial angles, we can control the force applied to CoboSkin. An impact force sensor connected with a data acquisition (DAQ) board was attached to the frame, and the photoelectric gate was used to detect the impact speed. The schematic illustration of the collision test setup for evaluating the performance of CoboSkin is shown in Figure 8a (see more details in Section 4). The resulting impact forces were measured using a fixed force sensor, as shown in Figure 8b. As to the CoboSkin without internal air pressure, the impact peak force of the collision was 93 N. The impact peak force of

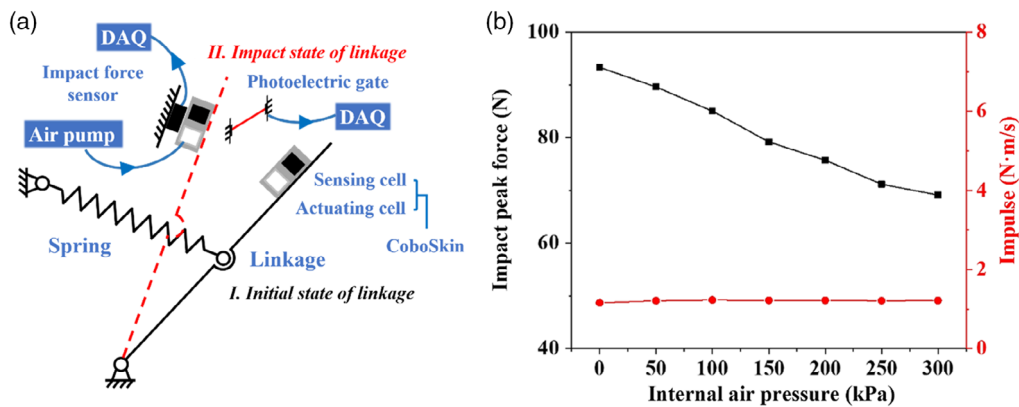


Figure 8. Collision test results of CoboSkin. a) Schematic illustration of the collision test setup for evaluating the performance of CoboSkin. DAQ means data acquisition card. b) Comparison between peak force and impulse with different internal air pressure force.

collision decreased to 69 N, when CoboSkin was filled with 300 kPa high-pressure gas, 26% smaller than the maximum impact peak force. Furthermore, we also collected the impact peak force time of collisions with seven internal air pressures. Table 2 shows that the impact peak force time is negatively correlated with the internal air pressure, which is also in line with the theorem of momentum. In this experiment, the impulse of the swing link is integrated, and the results are almost uniform, which means these collisions have the same impact energy. Therefore, this experiment confirms that CoboSkin can reduce the peak impact force by altering internal air pressure.

The simplified control strategy of CoboSkin is mainly up to the working speed of Cobots. To minimize the impact force, the skin should be softer when the working speed of the host robot is low. In contrast, it should be stiffer when the speed is high. These two factors (i.e., sensitivity and buffering capacity) cannot be controlled independently in the CoboSkin indeed. However, users usually touch robots for their interaction only when the robots move slowly. Accordingly, the CoboSkin can enhance the

Table 2. Time from start to peak in experiment varying with internal air pressure.

Internal air pressure [kPa]	0	50	100	150	200	250	300
Impact peak force time [ms]	12.8	13.2	13.4	13.5	13.7	13.8	14.0

sensitivity for sensing the user's touch (i.e., interactive force), and reduce the impact force without any conflict. When the operation speed of the host robot is high, we will enhance the buffering capacity for safety. In such a situation, the unintended collision force is high.

2.3. Adaptation to Off-the-Shelf Cobot System

2.3.1. Adaptation of Mechanical Design

In previous researches, the main challenge in applying soft skin to robot arms is to follow the complex contour and various shapes on the robot.^[23] To cope with this challenge, we tend to adopt the molding and foaming process to fabricate soft skin that has complex geometry features. First, we can construct sophisticated digital models of molds that can be directly integrated on robot surfaces and then fabricated designed molds by leveraging 3D printing technology. After deploying all units on 3D-printed molds, we can fabricate the soft skin through the foaming process, which is able to be integrated on YuMi's arm where the shapes and contour are complex. We believe this method is feasible because we have already applied the skin manufactured by this method to one of the contours on YuMi robot's arm. Figure 9a shows the complex contour of the robot's arm and how we design the CoboSkin carrier. In Figure 9b, we have fabricated the

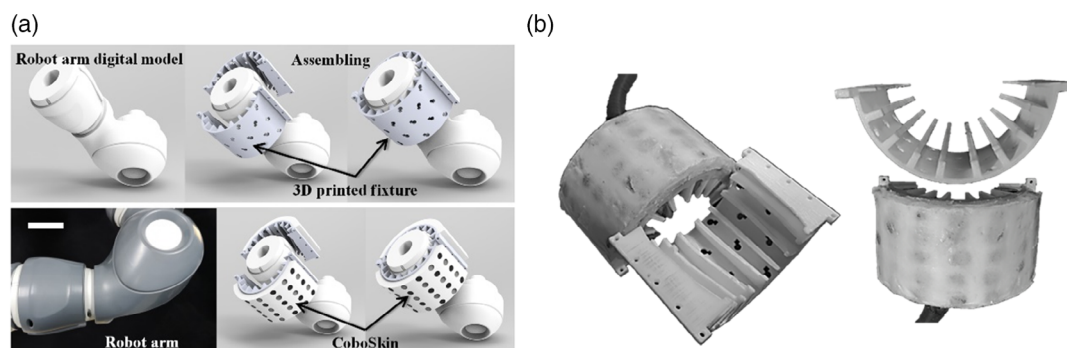


Figure 9. Robotic links of ABB YuMi Cobot integrated with CoboSkin. a) Schematic of digital models of CoboSkin and 3D-printed integration devices. Scale bar: 5 cm. b) Photographs of CoboSkin and 3D-printed integration devices.

CoboSkin for “YuMi” robot. This prototyping and integration method can also be used in other robots, as long as we have 3D models of parts, where we want to install the CoboSkin on the robot.

2.3.2. Integration of Control System

Utilizing the equipotential shielding method and voltage divider rule, a read-out circuit had been built to collect the raw data of sensing elements in CoboSkin. The raw data was

packaged and transferred by an Arduino through the integrated analog-to-digital converter (ADC). The digital voltage signals were sent to a personal computer (PC) (or YuMi Robot) through the serial interface. To inflate pneumatic actuating cells, compressed air was provided by a compressive air pump, as shown in **Figure 10a**. The solenoid valve was controlled by pulse-width-modulation (PWM). Precision pressure sensors were used to control and maintain the internal air pressure in the CoboSkin. In addition, we built a communication platform

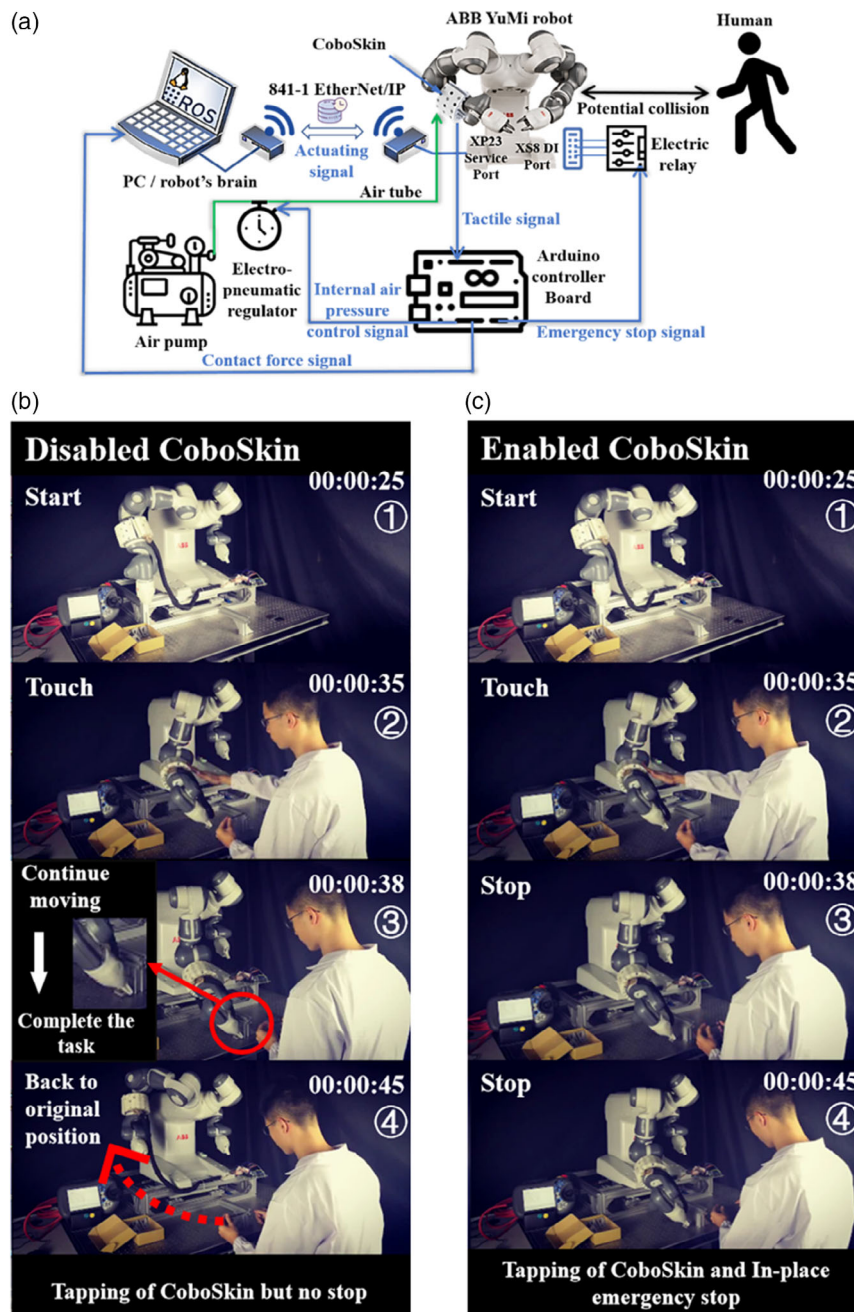


Figure 10. The adaption of CoboSkin to the physical and control system. a) DAQ and control system of CoboSkin. b) The practical situation of disabled CoboSkin for YuMi robot in HRC. (Flow: Start–Touch–Continue moving–Complete the task–Back to original position). c) The practical situation of disabled CoboSkin for YuMi robot in HRC. (Flow: Start–Touch–Stop).

between the robot's controller and an external PC installed with the Ubuntu operation system and the Robot Operation System (ROS). It should be clarified that the control framework of the YuMi robot in this work is based on ROS, which is a flexible and distributed framework designed for robot control. The communication between YuMi robot and the external PC was established by Ethernet. In terms of the robot's controller, we developed programs for ABB YuMi robot based on the specialized RAPID language. In ROS, we mainly designed programs for the corresponding control node through Python and C++ Programming Language. In this work, an Arduino board was used to collect the CoboSkin's signal and connected to the XS8 DI port of YuMi robot's controller to trigger an interrupt signal. Moreover, the Unified Robot Description Format (URDF) model in ROS must be updated and the corresponding collision matrix should be created to avoid the interference introduced by the thickness of CoboSkin.

To demonstrate the DAQ system can work in HRC, we experimented with both enabled and disabled CoboSkin. The host robot of this experiment is ABB YuMi robot, which has a self-detection system for current from torque sensors that are embedded into the joints of YuMi robot. We contrasted the perception ability of the developed CoboSkin and the built-in sensors of YuMi robot in the situation of HRC for fixing the mounting bracket. As shown in Figure 10b,c, these two sets of photos were recorded at the same timeline. The left one showcased the scenario where the CoboSkin on the robot is disabled. In such a situation, the volunteer touched the CoboSkin on the robot, while the robot did not stop and continued moving until finishing the preset task trajectories, because the touch did not trigger the original sensor and CoboSkin in YuMi robot. Then the arm of the robot retracted and was back to the original position. There is no human–robot interaction during this entire process. This experiment showed that YuMi without CoboSkin has defects in force detection in HRC. The right one demonstrates the scenario where the CoboSkin on the robot is enabled. When the volunteer touched the CoboSkin, aiming to stop the potential collision with the robot peer, the robot stopped on-site in time, and it took 0.73 s from the moment the volunteer touched the robot to the moment the robot stopped. These 0.73 s included the transmission time of the read-out circuit, the computational duration of resistance data, and the program execution time of robot control. In this experiment, we defined that the robot stops if a human touches the link of YuMi arms with CoboSkin which is a common control signal of human–robot interaction. The result was what we defined and expected. The comparison of these two sets indicated that robots with CoboSkin could be integrated on robots both in a physical system and in a control system, detect force information from the external environment to enhance the coordination between human and robot.

2.3.3. Comparison of Minimum Detectable Force

To measure the minimum detectable force of YuMi robot, we have built the experimental setup to measure the parameter by an impact force sensor at the same contact position on the robot arm with CoboSkin, as the force value cannot be given

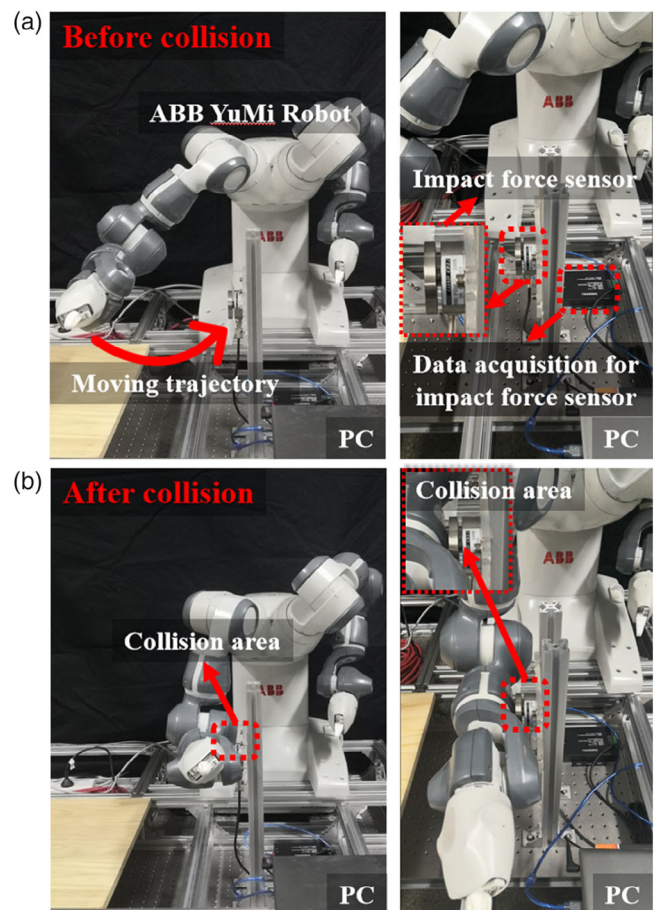


Figure 11. Experimental setup for measuring the minimum detectable force of YuMi robot without CoboSkin. a) Experiment before the collision. b) Experiment after the collision.

directly by the robot. The experimental setup is demonstrated in **Figure 11**, where we altered the parameters of YuMi robot, including the motion supervision level (i.e., the sensitivity to collision force) of Collision Detection (i.e., the self-integrated collision detection module) and the speed of tool center point (TCP) of end-effector. The motion supervision level is 100% by default, and users can change it from 1% to 300%. The lower percentage of the motion supervision level the user set, the higher the sensitivity of collision detection the robot will have.

The test results of the minimum detectable force of YuMi robot in different conditions are summarized in **Table 3**. The overall minimum detectable force was 5.125 N, when the motion supervision level and TCP velocity were set as 60% and 2 mm s^{-1} , respectively. Compared with YuMi robot, the developed CoboSkin were able to provide host robot with a much lower detectable force (0.1 N) to enhance the safety performance in HRC.

We have experimented on the minimum detectable force with a single functional module of CoboSkin, as shown in **Figure 12**. To measure the minimum detectable force of the functional units, we applied a cyclic force from 0 to 0.1 N to a single functional module by the test machine at a loading speed of

Table 3. Stopped collision force of YuMi robot without CoboSkin.

Motion supervision level [%]	The speed of TCP of end-effector							
	2 [mm s ⁻¹]	10 [mm s ⁻¹]	50 [mm s ⁻¹]	100 [mm s]	250 [mm s]	500 [mm s ⁻¹]	1000 [mm s ⁻¹]	1500 [mm s ⁻¹]
1–40	The robot arm was unable to move and stopped by inherent resistant force							
60	5.125 N	7.334 N	The robot arm was unable to move and stopped by inherent resistant force					
80	7.334 N	2.567 N	The robot arm was unable to move and stopped by inherent resistant force					
100	9.123 N	11.673 N	26.216 N	40.870 N	45.876 N	45.646 N	45.697 N	42.295 N
140	11.970 N	15.085 N	30.437 N	42.339 N	42.620 N	42.620 N	42.601 N	42.597 N
180	14.933 N	18.119 N	33.496 N	42.405 N	42.598 N	42.597 N	42.666 N	42.588 N
220	17.092 N	19.962 N	37.832 N	42.434 N	42.652 N	42.545 N	42.622 N	42.702 N
260	19.612 N	23.326 N	42.234 N	42.804 N	42.804 N	42.404 N	42.614 N	42.575 N
300	23.028 N	27.206 N	42.618 N	42.618 N	42.616 N	42.485 N	42.760 N	42.760 N

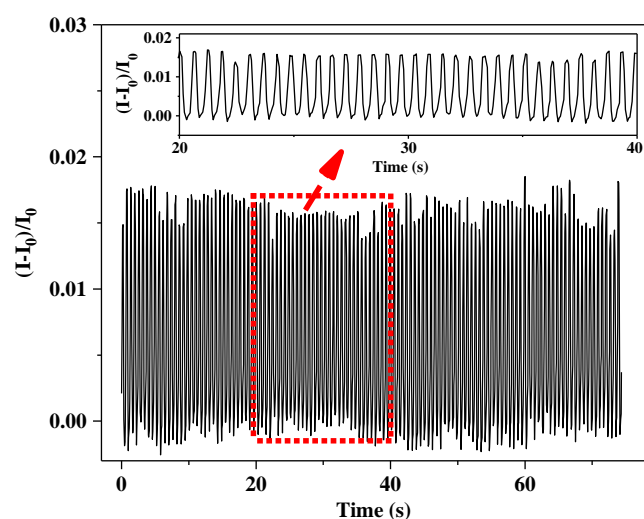


Figure 12. Electrical response of CoboSkin under 0.1 N dynamic force.

100 mm min⁻¹. The minimum loading limitation of the test machine is 0.1 N, which means that the potential minimum detectable force of proposed skin was blocked by the test machine rather than itself. The functional module had a good reproducibility in the test force range, illustrating that the minimum detectable force could be regarded as 0.1 N.

These two aforementioned experiments have demonstrated that the sensitivity of CoboSkin is 50 times higher than the sensors in the YuMi robot itself, which show us a promising future of CoboSkin on robot application.

3. Conclusion

In summary, a bionomic fluid-driven soft robot skin with adjustable stiffness in more than ten times and sensitivity in more than ten times was designed and fabricated. The CoboSkin, an integration of soft actuating cells and flexible sponge force sensors, exhibits multi-functions, including actuating and lifting, reducing the peak force of a collision, and actively altering sensitivity and detection range. In addition, the novel foaming process connecting these functional units in CoboSkin also

provides a method for the fabrication of flexible components in the future. Furthermore, we designed a method to integrate the CoboSkin on Cobots, developed a read-out circuit to get detection data from CoboSkin sensing array, and compared the minimum detectable force of YuMi robot with that of CoboSkin. The result shows that CoboSkin is 50 times more sensitive than the original sensors in YuMi robot. This work can be applied toward human–robot safe interaction and collaboration in the future.

4. Experimental Section

Fabrication of Pneumatic Actuating Cell: The internal part of the pneumatic actuating cell was made by silicon rubber (Ecoflex 00-30, Smooth-On, Macungie, PA, USA), and the outside part of the pneumatic actuating cell was made of inelastic nylon textile. First, silicon rubber solidified in a 3D-printed mold to make components of the internal part of the pneumatic actuating cell. Then, these components were glued together using silicone adhesives (Sil-Poxy, Smooth-On). Subsequently, the inelastic nylon textile was used to cover the internal part, and could be fixed using a cable tie.

Fabrication of Piezoresistive Sensing Cell: Commercially available PU foam (thickness: 10 mm) was cut into small cylindrical units (diameter: 10 mm) through laser cutting, followed by dipping coating in *n*-hexane suspension of CB (Mass ratio: *n*-hexane: CB = 20:1). Finally, these PU foam units were heated in a drying oven (100 °C, 2 h).

Fabrication of CoboSkin: Pneumatic actuating cells and piezoresistive sensing cells were spaced evenly in the mold (the distance between two cells: 5 mm). Then, we used copper wire with a diameter of 0.4 mm as the electrodes of the pressure-sensitive foam sensor. Finally, the PU foaming process (FlexFoam-iT III, Smooth-On) was performed in the mold. One hour later, CoboSkin disengaged from the mold.

Characterization of Sensing and Actuating Function: The external force and strain were applied and recorded by a digital tension and compression testing machine (ZQ-990B, Zhiqu Precision Instrument Co., Ltd., Dongguan, China). The 5 V constant voltage was supplied by a signal generator (2231A-30-3_287184, Tektronix Inc., Shanghai, China). The electrical response of the CoboSkin was recorded by a digital multimeter (Truevolt 34461A, Keysight Tech., Shanghai, China). The high-pressure compressed air was supplied by an air pump, and the internal air pressure was controlled by an electromagnetic solenoid valve (ITV1030, SMC Co., Ltd., Hangzhou, China). All these data were collected and processed by a PC. The subject of Section 2.1.2 was a sponge-sensing cell (height: 10 mm, diameter: 10 mm). The subject of Section 2.1.3 was a pneumatic actuating cell (height: 10 mm, diameter: 10 mm). The subject of Section 2.2.2 and

2.2.3 was a CoboSkin unit, which integrated one sponge-sensing cell and one pneumatic actuating cell (height: 30 mm, width: 15 mm, thickness: 10 mm).

Collision Test for Characterization of Safety Performance: The functional module was attached to a hinged linkage structure at a distance of 38 cm from the rotation center to mimic the robot link with a single degree of freedom. A controllable and repeatable collision model (e.g., impact velocity and impact force) was applied to the module by pulling and releasing the link in an adjustable initial state to impact a force sensor (NOS-F306, Nos-sensor, Changsha, China) through the tension spring. The mass of the link was 1.426 kg. The resulting impact forces were measured by the force sensor and collected through a DAQ board (NOS-FVA200, Nos-sensor) at a sampling rate of 30 kHz. To obtain the impact velocity, a pair of optoelectronic sensors (E3Z-T81, OMRON, Kyoto, Japan) was assembled on the top of test platform, located at a distance of 55 cm from rotation center, to detect the interruption time of light source when the link with a width of 3 cm passed the optoelectronic sensors and impacted the force sensor in the impact state, simultaneously. A DAQ board (NI USB 6002, National Instruments, Texas, USA) was used to monitor the signal from optoelectronic sensors at a sampling rate of 25 kHz.

The experiments involving human subjects have been performed with the full, informed consent of the volunteers, in accordance with all local laws and approved by the First Affiliated Hospital of Zhejiang University.

Supporting Information

Supporting Information is available from the Wiley Online Library or from the author.

Acknowledgements

W.H. and G.P. contributed equally to this work and should be considered co-first authors. This work was supported by the National Natural Science Foundation of China under Grant 51975513, the Major Research Plan of National Natural Science Foundation of China under Grant 51890884, the Natural Science Foundation of Zhejiang Province, China under Grant LR20E050003, the Zhejiang University Special Scientific Research Fund for COVID-19 Prevention and Control under Grant 2020XGZX017, the Director Foundation of the State Key Laboratory of Fluid Power and Mechatronic Systems under Grant SKLoFP_ZZ_2002, the Science Fund for Creative Research Groups of the National Natural Science Foundation of China under Grant 51821093, Robotics Institute of Zhejiang University under Grant K18-508116-008-03, and China's Thousand Talents Plan Young Professionals Program.

Conflict of Interest

The authors declare no conflict of interest.

Keywords

human-robot collaborations, safety, sensitive robot skin, soft actuators, three-dimensional printing

Received: March 9, 2020

Revised: May 7, 2020

Published online: July 8, 2020

[1] A. Cencen, J. C. Verlinden, J. M. P. Geraedts, *IEEE/ASME Trans. Mechatronics* **2018**, 23, 1092.

- [2] D. F. Paez Granados, B. A. Yamamoto, H. Kamide, J. Kinugawa, K. Kosuge, *IEEE Robot. Autom. Lett.* **2017**, 2, 1452.
- [3] Z. Pang, G. Yang, R. Khedri, Y. T. Zhang, *IEEE Rev. Biomed. Eng.* **2018**, 11, 249.
- [4] G. Yang, G. Pang, Z. Pang, Y. Gu, M. Mantysalo, H. Yang, *IEEE Rev. Biomed. Eng.* **2019**, 12, 34.
- [5] W. Heng, G. Pang, F. Xu, X. Huang, Z. Pang, G. Yang, *Sensors* **2019**, 19, 5197.
- [6] J. I. Furukawa, T. Noda, T. Teramae, J. Morimoto, *IEEE Trans. Robot.* **2017**, 33, 846.
- [7] T. Kim, J. Park, S. J. Yoon, D. H. Kong, H. W. Park, Y. L. Park, in *IEEE Int. Conf. on Soft Robotics (RoboSoft)*, IEEE, Seoul **2019**, pp. 257–264.
- [8] K. Schmid, H. Hirschmuller, in *IEEE Int. Conf. on Robotics and Automation*, IEEE, Karlsruhe, Germany, **2013**, pp. 4671–4678.
- [9] D. Hughes, J. Lammie, N. Correll, *IEEE Robot. Autom. Lett.* **2018**, 3, 1386.
- [10] T. J. Lee, C. H. Kim, D. I. D. Cho, *IEEE Trans. Ind. Electron.* **2019**, 66, 318.
- [11] S. Robla-Gomez, V. M. Becerra, J. R. Llata, E. Gonzalez-Sarabia, C. Torre-Ferrero, J. Perez-Oria, *IEEE Access* **2017**, 5, 26754.
- [12] K. Hosoda, Y. Tada, M. Asada, in *IEEE Int. Conf. on Intelligent Robots and Systems*, IEEE, Lausanne **2002**, pp. 111–115.
- [13] G. Cheng, E. Dean-Leon, F. Bergner, J. R. G. Olvera, Q. Leboutet, P. Mittendorfer, *Proc. IEEE* **2019**, 107, 2034.
- [14] G. Pang, J. Deng, F. Wang, J. Zhang, Z. Pang, G. Yang, *Micromachines* **2018**, 9, 576.
- [15] T. Kim, S. J. Yoon, Y. L. Park, *IEEE Robot. Autom. Lett.* **2018**, 3, 3216.
- [16] T. Matsuno, Z. Wang, K. Althoefer, S. Hirai, *IEEE Robot. Autom. Lett.* **2019**, 4, 2212.
- [17] Y. She, H. J. Su, D. Meng, S. Song, J. Wang, *J. Mech. Robot.* **2018**, 10, 1.
- [18] V. Villani, F. Pini, F. Leali, C. Secchi, *Mechatronics* **2018**, 55, 248.
- [19] J. J. Park, S. Haddadin, J. B. Song, A. Albu-Schäffer, in *IEEE Int. Conf. on Robotics and Automation*, IEEE, Shanghai **2011**, pp. 5413–5420.
- [20] B. Matthias, S. Kock, H. Jerregard, M. Källman, I. Lundberg, in *IEEE Int. Symp. on Assembly and Manufacturing*, IEEE, Tampere **2011**, pp. 1–6.
- [21] Y. Chen, M. Yu, H. A. Bruck, E. Smela, *Smart Mater. Struct.* **2016**, 25, 1.
- [22] G. Pang, G. Yang, W. Heng, Z. Ye, X. Huang, H. Yang, Z. Pang, *IEEE Trans. Ind. Electron.* **2020**, <https://doi.org/10.1109/TIE.2020.2978728>.
- [23] Y. Qiu, S. Ma, Q. Pei, J. D. Holbery, *Adv. Intell. Syst.* **2019**, 1, 1900054.
- [24] M. Fritzsche, N. Elkmann, E. Schulenburg, in *ACM/IEEE Int. Conf. Human-Robot Interaction IEEE*, Lausanne, **2011**, pp. 139–140.
- [25] S. Tsuji, T. Kohama, *IEEE Sens. J.* **2019**, 19, 5859.
- [26] S. Yao, P. Ren, R. Song, Y. Liu, Q. Huang, J. Dong, B. T. O'Connor, Y. Zhu, *Adv. Mater.* **2020**, 32, 1902343.
- [27] M. Manti, V. Cacucciolo, M. Cianchetti, *IEEE Robot. Autom. Mag.* **2016**, 23, 93.
- [28] S. Zhuo, Z. Zhao, Z. Xie, Y. Hao, Y. Xu, T. Zhao, H. Li, E. M. Knubben, L. Wen, L. Jiang, M. Liu, *Sci. Adv.* **2020**, 6, eaax1464.
- [29] S. Cheng, S. C. Gandevia, M. Green, R. Sinkus, L. E. Bilston, *J. Biomech.* **2011**, 44, 450.
- [30] T. P. Ho, K. Azar, S. Weinstein, W. W. Bowley, *J. Biomech.* **1982**, 15, 859.
- [31] X. Wu, Y. Han, X. Zhang, Z. Zhou, C. Lu, *Adv. Funct. Mater.* **2016**, 26, 6246.
- [32] Z. Ma, A. Wei, J. Ma, L. Shao, H. Jiang, D. Dong, Z. Ji, Q. Wang, S. Kang, *Nanoscale* **2018**, 10, 7116.
- [33] Y. Yang, Y. Song, X. Bo, J. Min, O. S. Pak, L. Zhu, M. Wang, J. Tu, A. Kogan, H. Zhang, T. K. Hsiai, Z. Li, W. Gao, *Nat. Biotechnol.* **2019**, 217, 38.
- [34] P. Polygerinos, N. Correll, S. A. Morin, B. Mosadegh, C. D. Onal, K. Petersen, M. Cianchetti, M. T. Tolley, R. F. Shepherd, *Adv. Eng. Mater.* **2017**, 19, 1.

- [35] J. Nassour, V. Ghadiya, V. Hugel, F. H. Hamker, in *IEEE Int. Conf. Soft Robotics* IEEE, Livorno **2018**, pp. 164–169.
- [36] L. Chen, W. Chen, Y. Xue, J. W. Wong, Y. Liang, M. Zhang, X. Chen, X. Cao, Z. Zhang, T. Li, *Extrem. Mech. Lett.* **2019**, *27*, 27.
- [37] R. Weitschat, J. Vogel, S. Lantermann, H. Hoppner, in *IEEE Int. Conf. on Robotics Automation* IEEE, Singapore, **2017**, pp. 2279–2284.
- [38] S. Kajita, R. Cisneros, M. Benallegue, T. Sakaguchi, S. Nakaoka, M. Morisawa, K. Kaneko, F. Kanehiro, in *IEEE-RAS Int. Conf. Humanoid Robots*, IEEE, Cancun **2016**, pp. 637–643.
- [39] V. Duchaine, N. Lauzier, M. Baril, M.-A. Lacasse, C. Gosselin, in *IEEE Int. Conf. on Robotics and Automation* IEEE, Kobe, **2009**, pp. 3676–3681.
- [40] Z. Jiao, C. Ji, J. Zou, H. Yang, M. Pan, *Adv. Mater. Technol.* **2019**, *4*, 1800429.
- [41] Q. Chen, J. Zhao, J. Ren, L. Rong, P. F. Cao, R. C. Advincula, *Adv. Funct. Mater.* **2019**, *29*, 1900469.
- [42] D. Gräfe, A. Wickberg, M. M. Zieger, M. Wegener, E. Blasco, C. Barner-Kowollik, *Nat. Commun.* **2018**, *9*, 1.
- [43] J. Morrow, H. S. Shin, C. Phillips-Graflin, S. H. Jang, J. Torrey, R. Larkins, S. Dang, Y. L. Park, D. Berenson, in *IEEE Int. Conf. on Robotics and Automation*, IEEE, Stockholm, **2016**, pp. 5024–5031.
- [44] S. S. Robinson, K. W. O'Brien, H. Zhao, B. N. Peele, C. M. Larson, B. C. Mac Murray, I. M. Van Meerbeek, S. N. Dunham, R. F. Shepherd, *Extrem. Mech. Lett.* **2015**, *5*, 47.